Eur. Phys. J. B **49**, 313–318 (2006)
DOI: 10.1140/epjb/e2006-00073-5

THE EUROPEAN PHYSICAL JOURNAL B

Exciton polaritons of nano-spherical-particle photonic crystals in compound lattices

Y. Zeng[1,2,a], X.S. Chen[1,b], W. Lu[1], and Y. Fu[2]

[1] National Laboratory for Infrared Physics, Shanghai Institute of Technical Physics, Chinese Academy of Science, 200083 Shanghai, China
[2] Theoretical Chemistry, Department of Biotechnology, Royal Institute of Technology, AlbaNova, 106 91 Stockholm, Sweden

Received 7 September 2005 / Received in final form 25 November 2005
Published online 10 March 2006 –

Abstract. Nonlocal investigations are presented for exciton-photon coupling in three-dimensional nano-spherical-particle photonic crystals in compound lattices for a tailored dielectric environment to optimize the optical properties of nano particles. The photonic band structure can be modified by tuning the nano particle size and the distance between two interlacing identical face-centered sub-lattices making up the photonic crystal lattice. A complete photonic band gap with a gap-midgap ratio as large as 40.82% has been found in the wurzite structure under the current investigation.

PACS. 42.70.Qs Photonic bandgap materials (for photonic crystal lasers, see 42.55.Tv) – 73.63.Kv Quantum dots – 41.20.-q Applied classical electromagnetism

Photonic crystals (PC) have attracted much attention in the last decade due to their unique electromagnetic (EM) properties and potential applications [1–4]. Conventional PCs consist of periodical dielectric arrays, which are normally referred to as passive PCs. One of their important properties is to mould and control the flow and distribution of the light at its most microscopic level. The synergetic interplay in these PCs between the microcavity resonances of composite particles and the Bragg scattering resonances of the dielectric arrays lead to the formation of a photonic band gap (PBG), i.e., a range of frequencies for which no propagating EM modes are allowed. Due to the presence of the PBG in the dispersion relation of the EM field, the photonic density of states (DOS) in PCs is suppressed over a certain frequency window. These features open the possibility for many important technological applications including lossless PC waveguides [4], low-threshold PC lasers [5], and high-Q photonic nanocavities [6].

Control of spontaneous emission lies at the heart of quantum optics. It has been well established over the years that the spontaneous emission of an excited atom depends not only on the properties of the excited atom, but also on the nature, i.e., the density of EM modes, of the surrounding environment [7]. For novel quantum-optics applications, a suitably tailored dielectric environment is required, where the vacuum fluctuations can be manipulated. PCs are exactly this, as they strongly modify the vacuum fluctuations, and accelerate or decelerate the decay of the emitted light [8]. There has been considerable experimental work reported recently on excited quantum dots (QDs) embedded in optical PCs by utilizing the properties of individual QD as well as the "colored" EM reservoir within the PCs [9–11]. Many new physical phenomena have been observed in these systems, such as the suppression and enhancement of spontaneous emission, anomalous superradiant emission, as well as vacuum Rabi splitting. For example, the light emission from a QD within an inverse opal PC is clearly modified [10].

A periodic QD array can form a photonic crystal due to Bragg scattering of optical waves in the structure. Optical properties of quantum wells were studied [12–14]. By state-of-the-art self-assembly techniques, Vlasov and coworkers have successfully fabricated high-quality three-dimensional (3D) QD PCs recently, and the promising experimental data indicated a complete PBG at optical wavelengths [15]. An interesting question has therefore arisen, namely whether we can utilize the QD array as a PC which in turn controls the light emission of the composite QDs.

As mentioned earlier, the PBG of a conventional PC is the result of the microcavity resonances of composite particles and the Bragg scattering resonances of the dielectric arrays. However, the EM field in the QD PCs is further modulated by the periodical coupling between light

[a] e-mail: yongzeng@mail.sitp.ac.cn
[b] e-mail: xschen@mail.sitp.ac.cn

and QD excitations [16–18]. Due to the quantum confinement effect, an exciton, a quantum of electronic energy, can be optically excited in these materials by the propagating EM waves. When a photon and an exciton mix in the dispersion-crossover region, a combined quasi-particle called an exciton polariton is formed [19]. For example, Ivchenko et. al. have studied exciton polaritons in one-dimensional (1D) PCs [14]. It was found that PBG can exist even in the absence of a periodically modulated dielectric index. When a photon is emitted from an excited QD in a QD PC, complex quantum-optics phenomena are expected. As a consequence of the formation of an exciton polariton, the photon DOS will be changed, which will cause the evolution of the excited QD, which in its turn will further modify the photon DOS again, and the process iterates until dynamic equilibrium is achieved.

Before an investigation of the complex system consisting of excited QDs in QD PCs, it is useful to first study the photonic band structure of QD PCs with exciton polaritons. After understanding the photonic band structures, one can further consider using such a PC to control the optical properties of the QDs. This question has been theoretically discussed by Fu and coworkers [20]. However, they did not find a complete PBG in either a primitive cubic lattice or a face-centered cubic (fcc) lattice. In this paper, we try to find a full PBG in 3D PC structures based on semiconductor-quantum-dot arrays in compound lattices. A complete PBG is obtained when the QDs are arranged in a wurtzite lattice. Moreover, we will formulate a complete theory about the polariton dispersion and optical spectrum of the QD PC in a general compound lattice.

The outline of this paper is as follows. Firstly, the dispersion equation for exciton polaritons in a 3D compound lattice will be derived. The compound structure is composed by two interlacing identical sublattices. One sublattice consists of QDs whose radii are R_1, the second sublattice have radii R_2. The photonic band structure of the PCs in compound lattices is then calculated. Finally, the numerical results are analyzed and discussed in comparison with the relevant results in reference [20].

We start from the Maxwell equations (without free charges and the current due to spatial transfer of free charges)

$$\nabla \times [\nabla \times \boldsymbol{E}(\boldsymbol{r})] = \left(\frac{\omega}{c}\right)^2 \boldsymbol{D}(\boldsymbol{r}),$$
$$\nabla \cdot \boldsymbol{D}(\boldsymbol{r}) = 0. \quad (1)$$

The excitonic states in a single QD are quasi-zero-dimensional due to the quantum-confinement effect and we consider a narrow frequency region near a particular exciton energy level, where the dielectric response to an electromagnetic wave is nonlocal. And the nonlocal relationship between $\boldsymbol{D}$ and $\boldsymbol{E}$ is taken in the form [21]

$$\boldsymbol{D}(\boldsymbol{r}) = \epsilon_b \boldsymbol{E}(\boldsymbol{r}) + 4\pi \boldsymbol{P}_{exc}(\boldsymbol{r}), \quad (2)$$

where ϵ_b is the dielectric index of the QD. To simplify the Maxwell equations, we neglect the tiny difference between dielectric indices of the well and barrier materials [14]. This assumption is realistic for many semiconductor materials such as III-V GaAs/Al_xGa_{1-x}As QDs. The dielectric polarization is given by

$$4\pi \boldsymbol{P}_{exc}(\boldsymbol{r}) = T(\omega)\left[\sum_{\boldsymbol{a}} \Phi_{1,\boldsymbol{a}}(\boldsymbol{r}) \int \Phi_{1,\boldsymbol{a}}(\boldsymbol{r'})\boldsymbol{E}(\boldsymbol{r'})d\boldsymbol{r'} + \sum_{\boldsymbol{a}+\Delta\boldsymbol{a}} \Phi_{2,\boldsymbol{a}+\Delta\boldsymbol{a}}(\boldsymbol{r}) \int \Phi_{2,\boldsymbol{a}+\Delta\boldsymbol{a}}(\boldsymbol{r'})\boldsymbol{E}(\boldsymbol{r'})d\boldsymbol{r'}\right]. \quad (3)$$

Here $\boldsymbol{a}$ are the sublattice primitive translation vectors, and $\Delta\boldsymbol{a}$ is the vector describing the distances between the two identical sublattices. $\Phi_{i,\boldsymbol{a}}(\boldsymbol{r}) = \Phi_{i,0}(\boldsymbol{r} - \boldsymbol{a})(i = 1, 2)$ is the envelope function of an exciton excited in the $\boldsymbol{a}$th QD. Other terms are

$$T(\omega) = 2\pi \frac{\epsilon_b \omega_{LT} \omega_0 a_B^3}{\omega_0^2 - \omega^2}, \quad (4)$$

ω_{LT} and a_B are the exciton longitudinal-transverse splitting and Bohr radius in the corresponding bulk semiconductor, ω_0 is the QD's exciton resonance frequency. Here, we assume the same resonant frequencies for two types of QDs with different sizes based on the fact that the QDs used in the current PC are relatively large. For instance, for QD PCs composed of GaAs QDs embedded in AlGaAs, the relative difference between excitonic resonant frequencies is of the order of 10^{-4} when we change the QD radius from 110 to 150 nm. In the following, we denote the composite quantum dots as nano spherical particles (NSPs) because of the large dot size. In addition, the distance between NSPs in the PC is large in order to localize the exciton. Thus, we neglect the overlap of the exciton envelope functions $\Psi_{i,\boldsymbol{a}}$ and $\Psi_{j,\boldsymbol{a'}}(i, j = 1, 2)$ with $\boldsymbol{a} \neq \boldsymbol{a'}$ and excitons excited in different NSPs are assumed to be coupled only via the EM field.

Notice that the non-radiative damping rate of the excited exciton state is neglected in equation (4), which is valid for frequencies away from the excitonic resonance frequency ω_0, where the non-radiative damping rates are very small. Because we just consider the frequency above ω_0 (see discussions below), the non-radiative damping rate can be reasonably neglected from the dielectric function. This is more clearly seen in the photonic band structure around the PBG of interest above ω_0 (see Figs. 2–4 below). However, when the frequencies are very close to ω_0, this assumption is no longer valid. Another thing needed to note is that the small non-radiative damping rate only has a very small effect on the band structure. It clearly affects both the electric field distribution and the spectrum.

It follows from equation (2) that $\mathrm{div}\boldsymbol{E} = -(4\pi/\epsilon_b)\mathrm{div}\boldsymbol{P}_{exe}$, which allows us to rewrite the first equation (1) as

$$\nabla^2 \boldsymbol{E}(\boldsymbol{r}) + k^2 \boldsymbol{E}(\boldsymbol{r}) = -4\pi k_0^2 \left\{\boldsymbol{P}(\boldsymbol{r}) + \frac{1}{k^2}\nabla\left[\nabla \cdot \boldsymbol{P}(\boldsymbol{r})\right]\right\}, \quad (5)$$

where $k_0 = \omega/c$, $k = k_0 n_b = \omega n_b/c$ and $n_b = \sqrt{\epsilon_b}$.

$$D_{6\times 6}=\begin{pmatrix} 1-R_{1,11} & -R_{1,12} & -R_{1,13} & -R_{2,11} & -R_{2,12} & -R_{2,13} \\ -R_{1,21} & 1-R_{1,22} & -R_{1,23} & -R_{2,21} & -R_{2,22} & -R_{2,23} \\ -R_{1,31} & -R_{1,32} & 1-R_{1,33} & -R_{2,31} & -R_{2,32} & -R_{2,33} \\ R_{3,11} & R_{3,12} & R_{3,13} & R_{4,11}-1 & R_{4,12} & R_{4,13} \\ R_{3,21} & R_{3,22} & R_{3,23} & R_{4,21} & R_{4,22}-1 & R_{4,23} \\ R_{3,31} & R_{3,32} & R_{3,33} & R_{4,31} & R_{4,32} & R_{4,33}-1 \end{pmatrix}. \quad (17)$$

We substitute equations (3) into (5) and expand the vector function $\boldsymbol{E_q}(\boldsymbol{r})$ in the Fourier series

$$\boldsymbol{E_q}(\boldsymbol{r})=\sum_{\boldsymbol{g}} e^{i(\boldsymbol{q}+\boldsymbol{g})\cdot\boldsymbol{r}}\boldsymbol{E}_{\boldsymbol{q}+\boldsymbol{g}}, \quad (6)$$

$\boldsymbol{g}$ are the reciprocal lattice vectors. The integral in equation (3) can be transformed into

$$\int \Phi_{1,\boldsymbol{a}}(\boldsymbol{r})\boldsymbol{E}(\boldsymbol{r})d\boldsymbol{r}=e^{i\boldsymbol{q}\cdot\boldsymbol{a}}\sum_{\boldsymbol{g}} I_{1,\boldsymbol{q}+\boldsymbol{g}}\boldsymbol{E}_{\boldsymbol{q}+\boldsymbol{g}}\equiv e^{i\boldsymbol{q}\cdot\boldsymbol{a}}\boldsymbol{\Lambda_1}$$
$$\int \Phi_{2,\boldsymbol{a}+\Delta\boldsymbol{a}}(\boldsymbol{r})\boldsymbol{E}(\boldsymbol{r})d\boldsymbol{r}=e^{i\boldsymbol{q}\cdot\boldsymbol{a}}\sum_{\boldsymbol{g}} I_{2,\boldsymbol{q}+\boldsymbol{g}}\boldsymbol{E}_{\boldsymbol{q}+\boldsymbol{g}}\equiv e^{i\boldsymbol{q}\cdot\boldsymbol{a}}\boldsymbol{\Lambda_2}, \quad (7)$$

where

$$I_{1,\boldsymbol{q}+\boldsymbol{g}}=\int \Phi_{1,0}(\boldsymbol{r})e^{i(\boldsymbol{q}+\boldsymbol{g})\cdot\boldsymbol{r}}d\boldsymbol{r}$$
$$I_{2,\boldsymbol{q}+\boldsymbol{g}}=\int \Phi_{2,0}(\boldsymbol{r})e^{i(\boldsymbol{q}+\boldsymbol{g})\cdot\boldsymbol{r}}e^{i(\boldsymbol{q}+\boldsymbol{g})\cdot\Delta\boldsymbol{a}}d\boldsymbol{r}. \quad (8)$$

The sums $\sum_{\boldsymbol{a}}\Phi_{1,\boldsymbol{a}}(\boldsymbol{r})e^{i\boldsymbol{q}\cdot\boldsymbol{a}}$ and $\sum_{\boldsymbol{a}+\Delta\boldsymbol{a}}\Phi_{2,\boldsymbol{a}+\Delta\boldsymbol{a}}(\boldsymbol{r})e^{i\boldsymbol{q}\cdot\boldsymbol{a}}$ satisfy the translational symmetry and can be presented as

$$\sum_{\boldsymbol{a}}\Phi_{1,\boldsymbol{a}}(\boldsymbol{r})e^{i\boldsymbol{q}\cdot\boldsymbol{a}}=\sum_{\boldsymbol{g}} e^{i(\boldsymbol{q}+\boldsymbol{g})\cdot\boldsymbol{r}}\frac{I^*_{1,\boldsymbol{q}+\boldsymbol{g}}}{v_0}$$
$$\sum_{\boldsymbol{a}+\Delta\boldsymbol{a}}\Phi_{2,\boldsymbol{a}+\Delta\boldsymbol{a}}(\boldsymbol{r})e^{i\boldsymbol{q}\cdot\boldsymbol{a}}=\sum_{\boldsymbol{g}} e^{i(\boldsymbol{q}+\boldsymbol{g})\cdot\boldsymbol{r}}\frac{I^*_{2,\boldsymbol{q}+\boldsymbol{g}}}{v_0}, \quad (9)$$

where v_0 is the volume of the primitive unit cell. The system of linear equations for the space harmonics $\boldsymbol{E}_{\boldsymbol{q}+\boldsymbol{g}}$ can be written in the form

$$\left[|\boldsymbol{q}+\boldsymbol{g}|^2-k^2\right]\boldsymbol{E}_{\boldsymbol{q}+\boldsymbol{g}}=$$
$$k_0^2T(\omega)\left(\boldsymbol{\Lambda_1}\frac{I^*_{1,\boldsymbol{q}+\boldsymbol{g}}}{v_0}+\boldsymbol{\Lambda_2}\frac{I^*_{2,\boldsymbol{q}+\boldsymbol{g}}}{v_0}\right)\left[1-\frac{1}{k^2}(\boldsymbol{q}+\boldsymbol{g})^2\right]$$
$$=k_0^2T(\omega)\widehat{S}\left(\boldsymbol{\Lambda_1}\frac{I^*_{1,\boldsymbol{q}+\boldsymbol{g}}}{v_0}+\boldsymbol{\Lambda_2}\frac{I^*_{2,\boldsymbol{q}+\boldsymbol{g}}}{v_0}\right). \quad (10)$$

Here $\widehat{S}(Q)\boldsymbol{\Lambda_1}$ is a vector with the components $S_{\alpha\beta}\Lambda_{1,\beta}$ and $\widehat{S}(Q)\boldsymbol{\Lambda_2}$ is a vector with the components $S_{\alpha\beta}\Lambda_{2,\beta}$. We define $S_{\alpha\beta}=\delta_{\alpha\beta}-\frac{Q_\alpha Q_\beta}{k^2}$, where $\alpha,\beta=x,y,z$, $\delta_{\alpha\beta}$ is the Kronecker symbol. Dividing both parts of equation (10) by $\left[|\boldsymbol{q}+\boldsymbol{g}|^2-k^2\right]$, multiplying them by $I_{1,\boldsymbol{q}+\boldsymbol{g}}$ and summing over $\boldsymbol{g}$:

$$\sum_{\boldsymbol{g}} I_{1,\boldsymbol{q}+\boldsymbol{g}}\boldsymbol{E}_{\boldsymbol{q}+\boldsymbol{g}}=\boldsymbol{\Lambda_1}$$
$$=\frac{k_0^2T(\omega)}{v_0}\sum_{\boldsymbol{g}}\frac{\widehat{S}(\boldsymbol{q}+\boldsymbol{g})}{|\boldsymbol{q}+\boldsymbol{g}|^2-k^2}\left(|I_{1,\boldsymbol{q}+\boldsymbol{g}}|^2\boldsymbol{\Lambda_1}+I_{1,\boldsymbol{q}+\boldsymbol{g}}I^*_{2,\boldsymbol{q}+\boldsymbol{g}}\boldsymbol{\Lambda_2}\right)$$
$$=\widehat{R_1}(\omega,\boldsymbol{q})\boldsymbol{\Lambda_1}+\widehat{R_2}(\omega,\boldsymbol{q})\boldsymbol{\Lambda_2}, \quad (11)$$

where

$$\widehat{R_1}(\omega,\boldsymbol{q})=\frac{k_0^2T(\omega)}{v_0}\sum_{\boldsymbol{g}}\frac{\widehat{S}(\boldsymbol{q}+\boldsymbol{g})}{|\boldsymbol{q}+\boldsymbol{g}|^2-k^2}|I_{1,\boldsymbol{q}+\boldsymbol{g}}|^2$$
$$\widehat{R_2}(\omega,\boldsymbol{q})=\frac{k_0^2T(\omega)}{v_0}\sum_{\boldsymbol{g}}\frac{\widehat{S}(\boldsymbol{q}+\boldsymbol{g})}{|\boldsymbol{q}+\boldsymbol{g}|^2-k^2}I_{1,\boldsymbol{q}+\boldsymbol{g}}I^*_{2,\boldsymbol{q}+\boldsymbol{g}}. \quad (12)$$

Dividing both parts of equation (10) by $\left[|\boldsymbol{q}+\boldsymbol{g}|^2-k^2\right]$, multiplying them by $I_{2,\boldsymbol{q}+\boldsymbol{g}}$ and summing over $\boldsymbol{g}$:

$$\sum_{\boldsymbol{g}} I_{2,\boldsymbol{q}+\boldsymbol{g}}\boldsymbol{E}_{\boldsymbol{q}+\boldsymbol{g}}=\boldsymbol{\Lambda_2}$$
$$=\frac{k_0^2T(\omega)}{v_0}\sum_{\boldsymbol{g}}\frac{\widehat{S}(\boldsymbol{q}+\boldsymbol{g})}{|\boldsymbol{q}+\boldsymbol{g}|^2-k^2}\left(|I_{2,\boldsymbol{q}+\boldsymbol{g}}|^2\boldsymbol{\Lambda_2}+I_{2,\boldsymbol{q}+\boldsymbol{g}}I^*_{1,\boldsymbol{q}+\boldsymbol{g}}\boldsymbol{\Lambda_1}\right)$$
$$=\widehat{R_3}(\omega,\boldsymbol{q})\boldsymbol{\Lambda_1}+\widehat{R_4}(\omega,\boldsymbol{q})\boldsymbol{\Lambda_2}, \quad (13)$$

where

$$\widehat{R_3}(\omega,\boldsymbol{q})=\frac{k_0^2T(\omega)}{v_0}\sum_{\boldsymbol{g}}\frac{\widehat{S}(\boldsymbol{q}+\boldsymbol{g})}{|\boldsymbol{q}+\boldsymbol{g}|^2-k^2}I_{2,\boldsymbol{q}+\boldsymbol{g}}I^*_{1,\boldsymbol{q}+\boldsymbol{g}}$$
$$\widehat{R_4}(\omega,\boldsymbol{q})=\frac{k_0^2T(\omega)}{v_0}\sum_{\boldsymbol{g}}\frac{\widehat{S}(\boldsymbol{q}+\boldsymbol{g})}{|\boldsymbol{q}+\boldsymbol{g}|^2-k^2}|I_{2,\boldsymbol{q}+\boldsymbol{g}}|^2. \quad (14)$$

We arrive at the vector equations

$$\left(I-\widehat{R_1}(\omega,\boldsymbol{q})\right)\boldsymbol{\Lambda_1}=\widehat{R_2}(\omega,\boldsymbol{q})\boldsymbol{\Lambda_2}$$
$$\left(I-\widehat{R_4}(\omega,\boldsymbol{q})\right)\boldsymbol{\Lambda_2}=\widehat{R_3}(\omega,\boldsymbol{q})\boldsymbol{\Lambda_1}, \quad (15)$$

where I is a 3×3 unit matrix. We can rewrite the above equations as

$$D_{6\times 6}\boldsymbol{X}=0, \quad (16)$$

where

see equation (17) above

$\boldsymbol{X}$ is a column vector that can be transposed as

$$(\Lambda_{1,x}, \Lambda_{1,y}, \Lambda_{1,z}, \Lambda_{2,x}, \Lambda_{2,y}, \Lambda_{2,z})^T. \quad (18)$$

The exciton-polariton dispersion $\omega(\boldsymbol{q})$ satisfies the equation

$$Det\|D\| = 0. \quad (19)$$

Consider NSPs with radius R, where $R \gg a_B$ so that one may neglect the distortion of internal motion of the electron-hole pair in the exciton and the envelope function of an exciton can be approximated by the exciton ground state wavefunction [20,22]

$$\Psi_{\boldsymbol{a}}(\boldsymbol{r}_e, \boldsymbol{r}_h) = \frac{1}{|\boldsymbol{r}-\boldsymbol{a}|\sqrt{2\pi R}} \sin\left(\frac{\pi|\boldsymbol{r}-\boldsymbol{a}|}{R}\right) \frac{1}{\sqrt{\pi a_B^3}} e^{-\frac{r_e - r_h}{a_B}}, \quad (20)$$

where

$$\boldsymbol{r} = \frac{m_e \boldsymbol{r}_e + m_h \boldsymbol{r}_h}{m_e + m_h} \quad (21)$$

is the exciton center of mass. So we have

$$I_{1,\boldsymbol{Q}} = \pi \left(\frac{2R_1}{a_B}\right)^{3/2} \frac{\sin|\boldsymbol{Q}|R_1}{|\boldsymbol{Q}|R_1\left[\pi^2 - (|\boldsymbol{Q}|R_1)^2\right]}$$
$$I_{2,\boldsymbol{Q}} = e^{i\boldsymbol{Q}\cdot\boldsymbol{\Delta a}} \pi \left(\frac{2R_2}{a_B}\right)^{3/2} \frac{\sin|\boldsymbol{Q}|R_2}{|\boldsymbol{Q}|R_2\left[\pi^2 - (|\boldsymbol{Q}|R_2)^2\right]}. \quad (22)$$

We then obtain

$$R_{1,\alpha\beta}(\Omega, \boldsymbol{K}) = \frac{16}{\pi v_0} \frac{\omega_{LT} R_1^3}{\omega_0} \frac{\omega^2}{\omega^2 - \omega_0^2} \sigma_{11,\alpha\beta}(\Omega, \boldsymbol{K})$$
$$R_{2,\alpha\beta}(\Omega, \boldsymbol{K}) = \frac{16}{\pi v_0} \frac{\omega_{LT} (R_1 R_2)^{3/2}}{\omega_0} \frac{\omega^2}{\omega^2 - \omega_0^2} \sigma_{12,\alpha\beta}(\Omega, \boldsymbol{K})$$
$$R_{3,\alpha\beta}(\Omega, \boldsymbol{K}) = \frac{16}{\pi v_0} \frac{\omega_{LT} (R_1 R_2)^{3/2}}{\omega_0} \frac{\omega^2}{\omega^2 - \omega_0^2} \sigma_{21,\alpha\beta}(\Omega, \boldsymbol{K})$$
$$R_{4,\alpha\beta}(\Omega, \boldsymbol{K}) = \frac{16}{\pi v_0} \frac{\omega_{LT} (R_2)^3}{\omega_0} \frac{\omega^2}{\omega^2 - \omega_0^2} \sigma_{22,\alpha\beta}(\Omega, \boldsymbol{K}), \quad (23)$$

where

$$\sigma_{st,\alpha\beta}(\Omega, \boldsymbol{K}) = \sum_{\boldsymbol{b}} \frac{f(|\boldsymbol{b}+\boldsymbol{K}|R_s) f(|\boldsymbol{b}+\boldsymbol{K}|R_t) S_{\alpha\beta}(\boldsymbol{b}+\boldsymbol{K})}{\Omega^2 - \Omega^2(\boldsymbol{b}+\boldsymbol{K})} \times e^{i(s-t)(\boldsymbol{b}+\boldsymbol{K})\cdot\boldsymbol{\Delta a}},$$
$$f(x) = \frac{\pi^2 \sin x}{x(\pi^2 - x^2)}$$
$$\Omega = \frac{\omega}{\omega_0}$$
$$\Omega(\boldsymbol{Q}) = \frac{c|\boldsymbol{Q}|}{\omega_0 n_b}, \quad (24)$$

where $\alpha, \beta = x, y, z$, and $s, t = 1, 2$. Now we are ready to calculate the EM dispersion relation. For a better comparison, we consider similar parameters discussed in reference [20]. We assume $\omega_{LT} = 5.0 \times 10^{-4}\omega_0$ and set the sublattice's lattice constant a in the unit of a_{Br},

$$a_{Br} = \frac{c\pi}{\omega_0 n_b}. \quad (25)$$

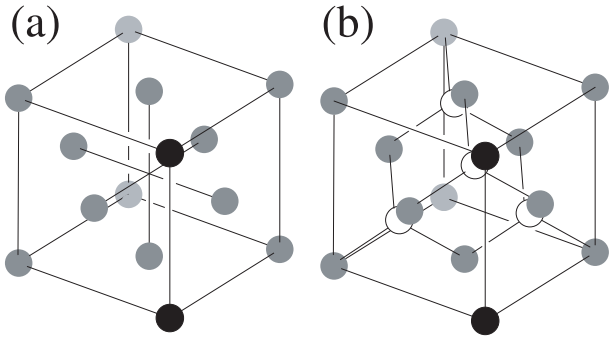

Fig. 1. Schematic of (a) a face-centered cubic lattice and (b) a wurtzite lattice.

We consider an fcc sublattice (schematically shown in Fig. 1a) since its Brillouin zone is most sphere-like and favourable for the overlapping of band gaps at various Brillouin-zone-boundary wave vectors [23]. In this lattice, the volume of the primitive unit cell is $v_0 = a^3/4$. For the fcc Bravais lattice with conventional cubic cell of size a, its reciprocal lattice is body-centered cubic, and the primitive reciprocal lattice vectors are [24]

$$\boldsymbol{b}_1 = \frac{2\pi}{a}(\boldsymbol{y}_0 + \boldsymbol{z}_0 - \boldsymbol{x}_0), \ \boldsymbol{b}_2 = \frac{2\pi}{a}(\boldsymbol{z}_0 + \boldsymbol{x}_0 - \boldsymbol{y}_0), \ \boldsymbol{b}_3 = \frac{2\pi}{a}(\boldsymbol{x}_0 + \boldsymbol{y}_0 - \boldsymbol{z}_0). \quad (26)$$

We calculate the photonic band structures for this structure along important symmetry lines in the Brillouin zone, $XU - UL - L\Gamma - \Gamma X - XW - WK$ (in unit of $2\pi/a$),

$$\Gamma = (0,0,0), \ X = (0,0,1), \ L = \left(\frac{1}{2}, \frac{1}{2}, \frac{1}{2}\right),$$
$$W = \left(\frac{1}{2}, 0, 1\right), U = \left(\frac{1}{4}, \frac{1}{4}, 1\right), K = \left(\frac{3}{4}, 0, \frac{3}{4}\right). \quad (27)$$

To validate the above equations and our calculating programs, we calculate the photonic band structures in two different conditions. One is an fcc sublattice of $\boldsymbol{\Delta a} = a(1/2, 0, 0)$, and the other is also fcc but $\boldsymbol{\Delta a} = a(1/2, 1/2, 1/2)$. They are equivalent in structure and the same results are obtained.

We first consider a NSP PC in a rock-salt lattice whose sublattices are composed of two kinds of NSPs, one with radius $a/4$ and the other $a/5$. The photonic band structure is shown in Figure 2 with the solid line. Up to $19 \times 19 \times 19$ plane waves have been used in the calculations, and a good convergence is achieved. Like the passive 3D fcc PC [3], our rock-salt lattice does not have a complete PBG. However, there is a large gap (from 0.365 to 0.384) between band 5 and 6 throughout most of the Brillouin zone. The distribution of mode frequencies around the W point prevents the gap from being complete. The partial gap is most prominent along the Λ (Γ-L) line in the $\boldsymbol{q}$ space. For comparison, the dispersion relationship of the fcc lattice with homogeneous QDs is also plotted [20]. Due to the change in structural symmetry, many splits appear in the band structure of our rock-salt lattice. Nevertheless, the

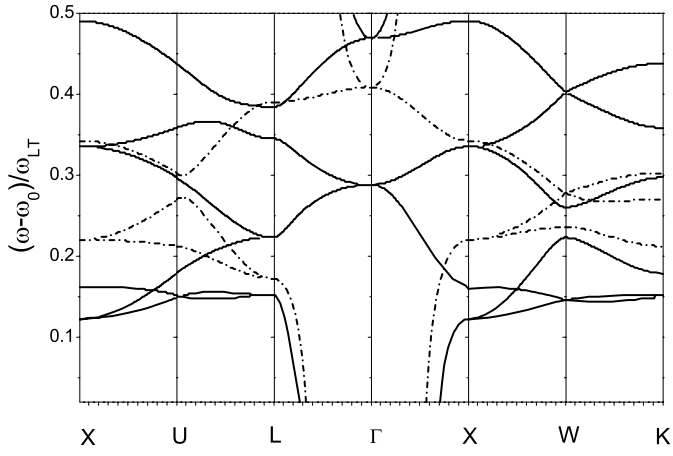

Fig. 2. Energy dispersion relation. $a = 0.95a_{Br}$ and $\omega_{LT}/\omega_0 = 5\times10^{-4}$. Solid line: a rock-salt lattice consisting of two kinds of nano-spherical particles with their radius equal to $a/4$ and $a/5$, respectively. Dotted line: a face-centered cubic lattice consisting of one kind of nano-spherical particle with radius $R = a/4$.

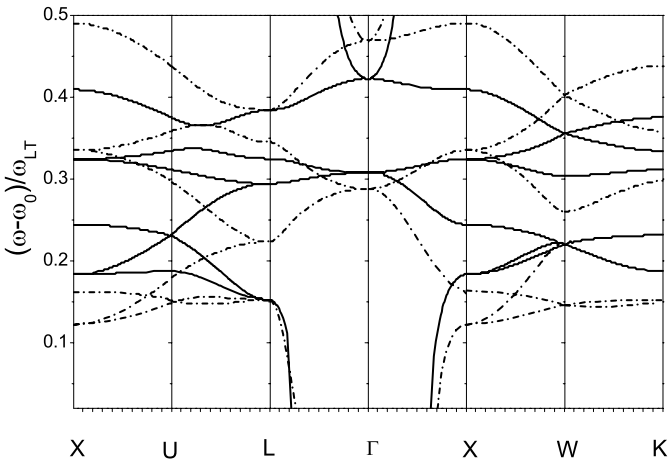

Fig. 3. Energy dispersion relations of two different rock-salt lattices consisting of two kinds of nano-spherical particles. The following values are assumed for the numerical calculation: $a = 0.95a_{Br}$, $\omega_{LT}/\omega_0 = 5\times10^{-4}$ and $\boldsymbol{\Delta a} = (1/2, 0, 0)a$. Solid line: rock-salt lattice with $R_1 = a/4, R_2 = a/8$; Dotted line: rock-salt lattice with $R_1 = a/4, R_2 = a/5$.

two band structures are sufficiently similar that a complete PBG is inhibited because of a symmetry-induced degeneracy at the W point.

In Figure 3 we show the photonic band structures of two different rock-salt lattices. The following values are assumed for numerical calculations: $a = 0.95a_{Br}$, $\omega_{LT}/\omega_0 = 5\times10^{-4}$ and $\boldsymbol{\Delta a} = (1/2, 0, 0)a$. The dotted line indicates the lattice with $R_1 = a/4$ and $R_2 = a/5$, while the solid line is for $R_1 = a/4$ and $R_2 = a/8$. These two lattices (identical except different NSP radii) do not have overall PBGs. In the first lattice, we find a partial band gap from 0.365 to 0.384. A large gap from 0.339 to 0.364 between band 5 and 6 throughout most of the Brillouin zone exists in the second lattice. In terms of the conclusion obtained in reference [20] that the dispersion relationship vertically shifts up along the $(\omega-\omega_0)/\omega_{LT}$-axis following the decrease of a/a_{Br} ratio, we further show here that the partial gap vertically shifts up following the increase of R_2. It is thus clearly concluded that we can undoubtedly change the photonic band structure by modifying the radius of NSPs in one sublattice.

Because of a symmetry-induced degeneracy at the W point, a complete PBG is inhibited in the above lattices. We therefore need to find ways to remove the degeneracy by changing the symmetry of the lattice. The next structure we try is a wurtzite lattice (schematically shown in Fig. 1b), where, like the diamond structure, all the bands along the symmetry line from W to X are twofold degenerate. This favours the opening of a gap between the second and third bands [3]. Figure 4 shows the photonic band structure of a wurtzite lattice, with $R_1 = 0.25a$ and $R_2 = 0.18a$. A complete PBG indeed appears clearly from 0.156 to 0.236, with the forbidden gap-midgap ratio of up to 40.82%. Several other important properties are also observed. First, there are extraordinarily flat bands, such as the second lowest band along the WK line, therefore the group velocity of these bands is extremely small. This property may be used for the development of efficient optical devices [3]. Secondly, several bands along the ΓX line are doubly degenerate, which is related to the symmetry of the lattice structure. Because EM waves are forbidden to propagate in any direction in the PBG, it can be expected that because of the intercoupling of light and NSPs [12,13], our NSP PC structure will undoubtedly enhance many novel quantum-optics phenomena such as photon localization, spontaneous emission and zero-point fluctuations [2].

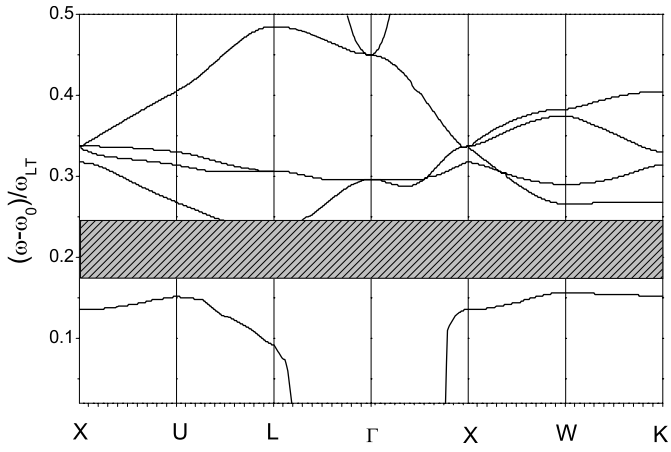

Fig. 4. Energy dispersion relation of a wurtzite structure consisting of nano-spherical particles. The following values are assumed for the numerical calculation: $a = 0.95a_{Br}$, $\omega_{LT}/\omega_0 = 5\times10^{-4}$, $\boldsymbol{\Delta a} = (1/4, 1/4, 1/4)a$, $R_1 = 0.25a$ and $R_2 = 0.18a$. The grey field indicates the forbidden gap.

Comparison between the photonic band structure of the wurtzite lattice in Figure 4 and that of the rock-salt lattice in Figure 3 clearly indicates a significant difference in the opening of the PBG. This phenomenon can be interpreted by the fact that the difference in the distance between two interlacing lattices leads to the variation of the

structural symmetry. We find that the opening of the band gap doesn't depend on the changes in the NSP radius. On the contrary, it depends on the distance between two interlacing sublattices. Hence, by modifying the distance to change the structural symmetry, we can effectively tune the photonic band structure for better performances of optical devices.

Coevorden et al. calculated the photonic band structure of fcc atomic lattices where the permeability, related to resonance frequency, was modelled by delta functions centered at the atomic sites [25]. A complete PBG was obtained in the fcc atomic lattices. The dielectric index is normally modelled by the resonance structure due to the light-matter interaction. The dielectric index is expected to be spatially distributed for a realistic composite particle. A 100-nm NSP under investigation contains more than 10^6 atoms in our NSP PC so that the dielectric index is expressed through the envelope function of the NSP exciton $\Phi(\boldsymbol{r})$. Moreover, the excitation of the exciton by the incident EM wave is included, i.e., the dependence of the dielectric index on the EM field, equation (3). We therefore see a significant difference in the photonic band structures of atomic and the NSP lattices. The complete PBG of the NSP PC is only obtained from complicated wurtzite lattices; it is not present in simple structures including primitive cubic and fcc lattices. In addition, the PBG in the NSP PCs is above the resonance frequency ω_0 (based on which the damping rate of the exciton state is neglected, see above), while it is almost below ω_0 in atomic lattices. Recently, many interesting results concerning NSP PC has been obtained [16–18].

In summary, we have studied the photonic band structure of the nano-spherical-particle photonic crystals in compound lattices and derived the dispersion equation using a plane-wave expansion method. The nano-spherical-particle photonics crystal can provide a tailored dielectric environment to optimize the optical properties of nano-spherical particles, such as the spontaneous emission. We have demonstrated for what we believe to be the first time that there is a complete photonic band gap with a large gap-midgap ratio in a nano-spherical-particle wurtzite lattice. By suitably choosing not only the nano-spherical particles' radius but also the distance between two interlacing sublattices, we can change the band-gap structure of this material.

This work is partially supported by Chinese National Key Research Special Fund, Chinese National Science Foundation (60221502 and 60476040), Key fund of Chinese National Science Foundation (10234040), Key Fund of Shanghai Science and Technology Foundation (02DJ14066).

References

1. E. Yablonovitch, Phys. Rev. Lett. **58**, 2059 (1987)
2. S. John, Phys. Rev. Lett. **58**, 2486 (1987)
3. J.D. Joannopoulos, R.D. Meade, J.N. Winn, *Photonic Crystals: Molding the Flow of Light* (Princeton university Press, New Jersey, 1995)
4. K. Sakoda, *Optical Properties of Photonic Crystals* (Springer, Berlin, 2001)
5. H.-G. Park, S.-H. Kim, S.-H. Kwon, Y.-G. Ju, J.-K. Yang, J.-H. Baek, S.-B. Kim, Y.-H. Lee, Science **305**, 1444 (2004)
6. Y. Akahane, T. Asano, B.-S. Song, S. Noda, Nature **425**, 944 (2003)
7. E.M. Purcell, Phys. Rev. **69**, 681 (1946)
8. Y. Zeng, X. Chen, W. Lu, Phys. Rev. E **70**, 047601 (2004)
9. T. Yoshie, A. Scherer, J. Hendrickson, G. Khitrova, H.M. Gibbs, G. Rupper, C. Ell, O.B. Shchekin, D.G. Deppe, Nature **432**, 200 (2004)
10. P. Lodahl, A.F. Driel, I.S. Nikolaev, A. Irman, K. Overgaag, D. Vanmaekelbergh, W.L. Vos, Nature **430**, 654 (2004)
11. E.P. Petrov, V.N. Bogomolov, I.I. Kalosha, S.V. Gaponenko, Phys. Rev. Lett. **81**, 77 (1998)
12. S. Nojima, Phys. Rev. B **59**, 5662 (1999)
13. S. Nojima, J. Phys. Soc. Jpn **70**, 3432 (2001)
14. E.L. Ivchenko, M.M. Voronov, M.V. Erementchouk, L.I. Deych, A.A. Lisyansky, Phys. Rev. B **70**, 195106 (2004)
15. Y.A. Vlasov, N. Yao, D.J. Norris, Adv. Mater. **11**, 165 (1999)
16. G. Ya. Slepyan, S.A. Maksimenko, V.P. Kalosha, A. Hoffmann, D. Bimberg, Phys. Rev. B **64**, 125326 (2001)
17. O. Voskoboynikov, C.M.J. Wijers, J.L. Liu, C.P. Lee, Phys. Rev. B **71**, 245332 (2005)
18. V. Bondarenko, M. Zaluzny, Y. Zhao, Phys. Rev. B **71**, 115304 (2005)
19. H. Haug, S.W. Koch, *Quantum Theory of the Optical and Electronic Properties of Semiconductors* (World Scientific, Singapore, 1986)
20. Y. Fu, M. Willander, E.L. Ivchenko, Superlatt. Microstruct. **27**, 255 (2000)
21. A. D'Andrea, R. Del Sole, Phys. Rev. B **25**, 3714 (1982)
22. E.L. Ivchenko, G.E. Pikus, *Superlattices and Other Heterostructures: Symmetry and Optical Phenomena* (Springer, Berlin, 1997)
23. K.M. Ho, C.T. Chan, C.M. Soukoulis, Phys. Rev. Lett. **65**, 3152 (1990)
24. C. Kittel, *Introduction to Solid State Physics* (John Wiley & Sons, New York, 1995)
25. D.V. van Coevorden, R. Sprik, A. Tip, A. Lagendijk, Phys. Rev. Lett. **77**, 2412 (1996)